Complimentary Surface Charge for Enhanced Capacitive Deionization

X. Gao,[a] S. Porada,[b] A. Omosebi,[a] K. Liu,[a,c,] P. M. Biesheuvel,[b,d] and J. Landon [a,]**

a: Center for Applied Energy Research, University of Kentucky, Lexington, Kentucky 40511, USA,

b: Wetsus, European Centre of Excellence for Sustainable Water Technology, Oostergoweg 9, 8911 MA Leeuwarden, The Netherlands,

c: Department of Mechanical Engineering, University of Kentucky, Lexington, Kentucky 40506, USA,

d: Laboratory of Physical Chemistry and Soft Matter, Wageningen University, Dreijenplein 6, 6703 HB Wageningen, The Netherlands,

*: Kunlei.Liu@uky.edu and James.Landon@uky.edu.

1. INTRODUCTION

Rapid growth in population, urbanization, and industrialization requires reliable water resources. Even though two-thirds of our world's surface is covered by water, only about 3% of that water can be directly consumed. Therefore, water quality and scarcity have become two of the most important global challenges of our time.(Elimelech and Phillip 2011, Schwarzenbach et al. 2010, Subramani and Jacangelo 2015) In addition to these issues, current water treatment standards such as multi-stage flash distillation and reverse osmosis are costly to implement and operate.(Avlonitis et al. 2003, Junjie et al. 2007) As a consequence, investigations into alternative desalination options are being explored in an effort to build sustainable water systems.(Suss et al. 2015)

Capacitive deionization (CDI) is a reversible adsorption desalination technology using highly porous carbon electrodes.(Anderson et al. 2010, Blair and Murphy 1960) By regulating applied voltages to a CDI cell, ionized salts can be trapped and released in the electric double layers (EDLs) at carbon electrodes, leading to water being desalinated through the use of a regenerative separation cell.(Farmer et al. 1996, Oren and Soffer 1978) Therefore, CDI technology may have potential advantages over current desalination methods in that no heat treatment or high pressure is required, which may lead to a significant decrease in the operational and energy costs compared to current desalination processes, aiding in the production of clean/fresh water.

In literature, although many experimental studies on CDI architectures (such as membrane-assisted CDI and flow-electrode CDI) and operational methods (such as constant-voltage and -current CDI operation) have been performed,(Bian et al. 2015, Gendel et al. 2014, Hatzell et al. 2014, Jande and Kim 2013, Lee et al. 2014, Omosebi et

al. 2015, Seo et al. 2010, Suss et al. 2012, Suss et al. 2015, Zhao et al. 2013), there is no doubt that salt removal of a CDI cell relies strongly on the physical and chemical properties of the carbon electrodes. For example, Porada *et al*. comprehensively studied the physical structure of carbon electrodes and concluded that the salt adsorption capacity could be dramatically improved with an increase in the carbon electrode's microporosity.(Porada et al. 2013) In addition to the porosity, Gao *et al.* examined carbon electrodes with enhanced chemical surface charge, leading to a recently developed inverted CDI process.(Gao et al. 2015b) Their work was preceded by many earlier studies regarding the potential of zero charge (E_{PZC}) and point of zero charge (pH_{PZC}).(Avraham et al. 2011, McCafferty 2010) Thus, there is clear evidence that both carbon porosity and chemical surface charge are among the most effective parameters for designing and preparing carbon electrodes for CDI applications.

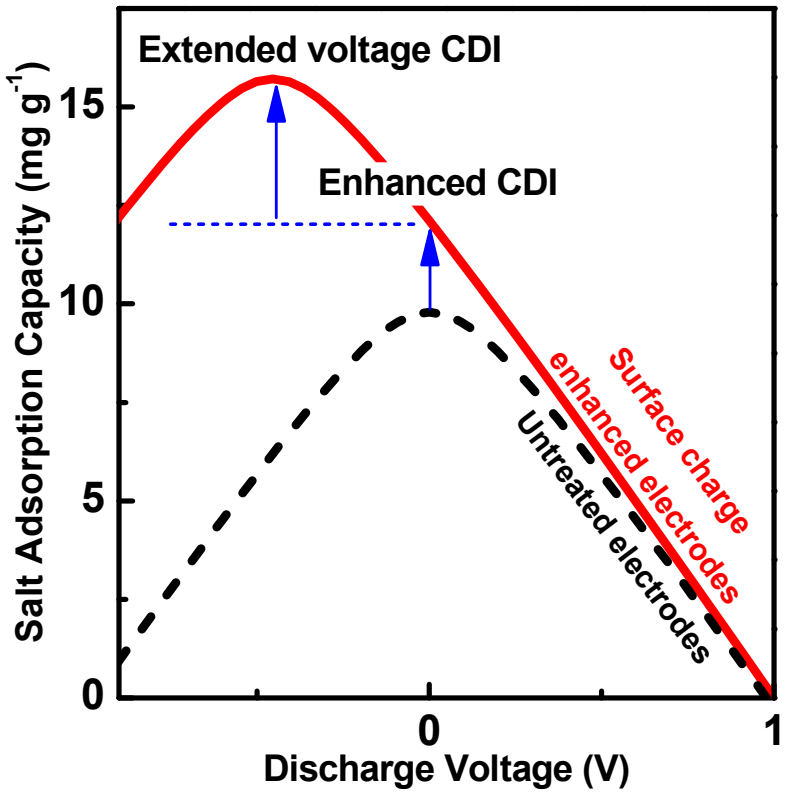

Figure 1. Predicted salt adsorption capacity (SAC) as a function of discharge voltage for a CDI cell. This prediction is performed using the amphoteric Donnan (amph-D) model when an influent salt concentration c_{inf} = 20 mM, Stern capacitance C_S = 170 F mL^{-1}, and charging voltage V_{ch} = 1.0 V. The black dashed line is a calculation for a CDI cell using untreated carbon electrodes with a chemical surface charge of 0 (zero) at both the anode and cathode, $\sigma_{chem,A} = \sigma_{chem,C} = 0$. The red solid line presents the result for a CDI cell using surface charge enhanced electrodes when $\sigma_{chem,A} = -\sigma_{chem,C} = 400$ mM. These parameters have been used in ref. (Biesheuvel et al. 2015).

Besides the various experimental works on carbon properties, theoretical studies have been performed to understand salt removal at the EDLs in carbon electrodes through the Gouy-Chapman-Stern and Donnan models.(Biesheuvel et al. 2014, Tang et al. 2015, Zhao et al. 2010) In particular, the Donnan model has been successfully used to describe salt adsorption and charge storage in CDI electrodes. Recently, combined with "chemical surface charge", the Donnan model is able to theoretically interpret the inverted CDI behavior observed from several experimental studies using different types of carbon electrodes.(Bouhadana et al. 2011, Cohen et al. 2011, Duan et al. 2015, Gao et al. 2014, Wu et al. 2015) This modified model is termed the amphoteric-Donnan (amph-D) model.(Biesheuvel 2015) As shown in Fig. 1, the amph-D model predicts salt removal behavior as a function of discharge voltage in a CDI cell. Interestingly, this prediction demonstrates that the use of surface charge enhanced electrodes results in an improved salt adsorption capacity, SAC, due to the "enhanced CDI" (e-CDI) effect, and additional improved SAC owing to the "extended voltage CDI" (eV-CDI) effect.(Biesheuvel et al. 2016, Biesheuvel et al. 2015)

In this paper, results are presented where commercially available carbon electrodes were treated using amine and acid solutions, resulting in both positive and negative surface charge enhanced electrodes. Through quantitative characterizations of both carbon pore volume and chemical surface charge for both the untreated and treated electrodes, we are for the first time experimentally demonstrating and validating both the enhanced SAC and extended working voltage window from predictions generated from the amph-D model. Based upon these combined experimental and theoretical studies, new insights will be provided on proper routes to characterize novel and functionalized

carbon electrodes for various CDI applications such as conventional, flow-electrode, membrane, and inverted CDI cells.

2. EXPERIMENTAL

2.1 Electrode Preparation - Pristine SpectraCarb (SC) (Engineered Fibers Technology, LLC, Connecticut, USA) electrodes were modified by nitric acid (70%, Sigma-Aldrich) and ethylenediamine (≥99%, Sigma-Aldrich) solutions resulting in the chemical surface charge of the electrodes being negatively and positively enhanced, respectively. Similar preparation has been introduced ref. (Yang et al. 2013). In our preparation, 30 g of as-received SC electrodes were placed into a container in which 400 mL of nitric acid was added. After immersion at room temperature for 24 hours, to remove any residual acid, the SC electrodes were washed with a significant amount of deionized water followed by drying at 280°C in air for 72 hours. Following on from the acid treatment, another glass container with 400 mL of N_2 purged ethylenediamine was heated to around 105°C in a silicone oil bath to further treat the acid-treated electrodes. This heating step was continued until all of the ethylenediamine solution completely evaporated. The carbon was further cleaned with deionized water, and subsequently dried at 105°C under N_2 atmosphere in a convection oven. To configure a conventional CDI cell, the nitric acid modified SC with negatively enhanced surface charge was used as the cathode (N-SC) while the ethylenediamine modified SC with positively enhanced surface charge was employed as the anode (P-SC).

2.2 Porosity and Surface Morphology - A porosity and surface area analyzer (ASAP2020, Micrometrics) was used to measure the N_2 adsorption-desorption isotherms for each sample. This measurement was carried out at 77 K using 0.1 g of sample degassed at

200°C overnight. The resulting isotherms were used to calculate the porosity of the electrodes through the non-localized density functional theory (NLDFT) provided by Micromeritics. In addition, a scanning electron microscope (SEM) (S-4800, Hitachi) was used to visualize the surface morphology of each sample.

2.3 Chemical Surface Charge and Surface Species - An automatic titration station (888 Titrando, Metrohm) was used to measure the acidic and basic surface properties of the samples. In this test, 0.5 g of carbon sample was first immersed in 50 mL of 0.05 M deaerated NaOH solution for several hours. To eliminate the influence of atmospheric CO_2, the test was conducted under gaseous N_2. The resulting NaOH solution with the carbon sample was slowly titrated by dosing 0.02 mL of 0.05 M HCl titrant every 3-5 min. To calculate the fixed chemical surface charge at the carbon surface, the above-mentioned procedure was repeated but without any carbon sample. Following the titrations, by the volume difference, Δv, in the titrant used with and without a sample at the same pH value, the fixed chemical surface charge per carbon micropore volume, σ_{chem}, was calculated via

$$\sigma_{\mathrm{chem}} = (\Delta v c)/v_{\mathrm{mi}} \qquad [1]$$

where c is the concentration of HCl used as titrant and v_{mi} is the measured micropore volume.(Babić et al. 1999, Noh and Schwarz 1990) A Fourier-transform infrared (FTIR) spectrometer (Nicolet 6700, Thermo Scientific) was used to identify surface species for each sample. FTIR samples were prepared with around 0.07 g of a mixture of carbon/KBr at a ratio of 0.3 wt% (SC *vs*. KBr), and FTIR spectra were collected by co-adding 256 scans at a resolution of 4 cm^{-1}.

2.4 CDI Experimental Procedure - To study the salt removal performance, a flow system was used, including a CDI cell, an in-line conductivity sensor, a peristaltic pump, and a polyethylene tank. In this system, a flow-by CDI cell was employed. The CDI cell structure and its components have been introduced in detail in ref. (Zhao et al. 2010). In this study, a single-pass mode was used to evaluate CDI performance. A large volume of solution of 5 mM deaerated NaCl was circulated through the CDI cell at a constant flow rate of 15 mL min^{-1}. Due to the large volume of NaCl solution used, the influent salt concentration at equilibrium, c_{inf}, after the adsorption and desorption profiles is approximately equivalent to the concentration of the initial bulk solution. As a consequence, the salt adsorption capacity, SAC or Γ, can be calculated by multiplying the volumetric flow rate, Φ, by the integration of the concentration curve with time, *t*, using

$$\Gamma = (M/m)\Phi \int (c(t) - c_{st})\mathrm{d}t \qquad [2]$$

where *M* is the molecular weight of NaCl (58.44 g mol^{-1}), and *m* is the total mass of the dry cathodes and anodes together used in the present tests. Similarly, the charge storage capacity, *Q*, for both the charging and discharging steps was calculated by integration of the current density curves stemming from the measured current divided by *m*. Finally, the charge efficiency, Λ, is

$$\Lambda = \Gamma F/M/Q \qquad [3]$$

where *F* is Faraday's constant (96485 C mol^{-1}).

3. THEORY

As indicated in refs (Biesheuvel et al. 2016, Biesheuvel et al. 2015), the Donnan model was modified by including immobile chemical surface charge to study salt removal of a CDI cell. In this modified model, by assumption, only the positive chemical charge is placed in the anode micropores while only the negative chemical charge is located in the cathode micropores. However, more realistically, due to the multiple-step treatments, several types of functional groups could be formed in the carbon micropores, some which may possess positive surface charges in one region and some which may have negative surface charges at another region. As a consequence, in ref. (Biesheuvel 2015), based upon the Donnan model including immobile chemical charge, the amph-D model was proposed by assuming the existence of both positive and negative surface charges at a carbon electrode.

In the amph-D model, mobile ionic charge due to cations and anions, $\sigma_{ionic,j}$, is balanced by not only electronic charge in the carbon matrix, $\sigma_{elec,j}$, but also immobile chemical surface charge, $\sigma_{chem,j}$ in the micropores at the carbon electrode, which is given by

$$\sigma_{ionic,j} + \sigma_{elec,j} + \sigma_{chem,j} = 0 \qquad [4]$$

where j represents the interfacial volumes in the carbon micropores. Based upon carbon surface chemistry, these interfacial volumes can be hypothetically divided into an acidic region, region A, with negative chemical surface charge, and a basic region, region B, with positive chemical surface charge, which has been schematically presented in the graphical abstract. As one example, the negative chemical surface charge can be due to the formation of acidic functional groups such as carboxylic groups. Likewise, the

positive chemical surface charge may be attributed to the attachment of amines and/or can be due to the carbon basal planes themselves.(Boehm 1994, Leon y Leon et al. 1992, Montes-Morán et al. 2004) In addition, it is assumed that both regions A and B exist in the micropores at both the cathode and anode, and all regions are described by Eq. 4. In this study, the net chemical surface charge for each electrode was estimated by a potentiometric titration method, which has been presented in the experimental section.

Following the inclusion of charge balance in the amph-D model, the Donnan and Stern potentials in each region, $\Delta\phi_{D,j}$ and $\Delta\phi_{S,j}$, for a 1:1 salt such as NaCl, at equilibrium, are given by

$$\Delta\phi_{D,j} = -\operatorname{arcsinh}\left(\sigma_{ionic,j}/2c_{inf}\right), \Delta\phi_{S,j} = (\sigma_{elec,j}F)/(C_S V_T) \quad [5]$$

where C_S is the capacitance of the Stern layer and V_T is the thermal voltage, where $V_T = RT/F$. More detailed descriptions regarding $\Delta\phi_{D,j}$ and $\Delta\phi_{S,j}$ can be found in ref. (Biesheuvel 2015). In the Donnan model, the total ion concentration in the micropores, $c_{ions,j}$, is given by

$$c_{ions,j}^2 = \sigma_{ionic,j}^2 + (2c_{inf})^2 \quad [6]$$

At the same electrode, regions A and B are coupled together via

$$c_{ions,mi} = \sum_{j=A,B} \alpha_j c_{ions,j}, \sigma_{elec} = \sum_{j=A,B} \alpha_j \sigma_{elec,j} \quad [7]$$

where $c_{ions,mi}$ is the micropore-averaged total ions concentration, α_j is the fraction of the total micropore volume, and σ_{elec} is the pore-averaged electronic charge density in the carbon electrode.

To solve the amph-D model, the values of $\sigma_{chem,j}$ in each region at each electrode and the value of C_S must be known. Furthermore, to convert calculated results to measurable properties such as the total charge passed and SAC values, a total micropore volume, v_{mi}, must be used, which is typically based on the experimentally obtained cumulative pore volume, see Fig. 2(b). Details of calculations using the amph-D model are also presented in ref. (Biesheuvel 2015).

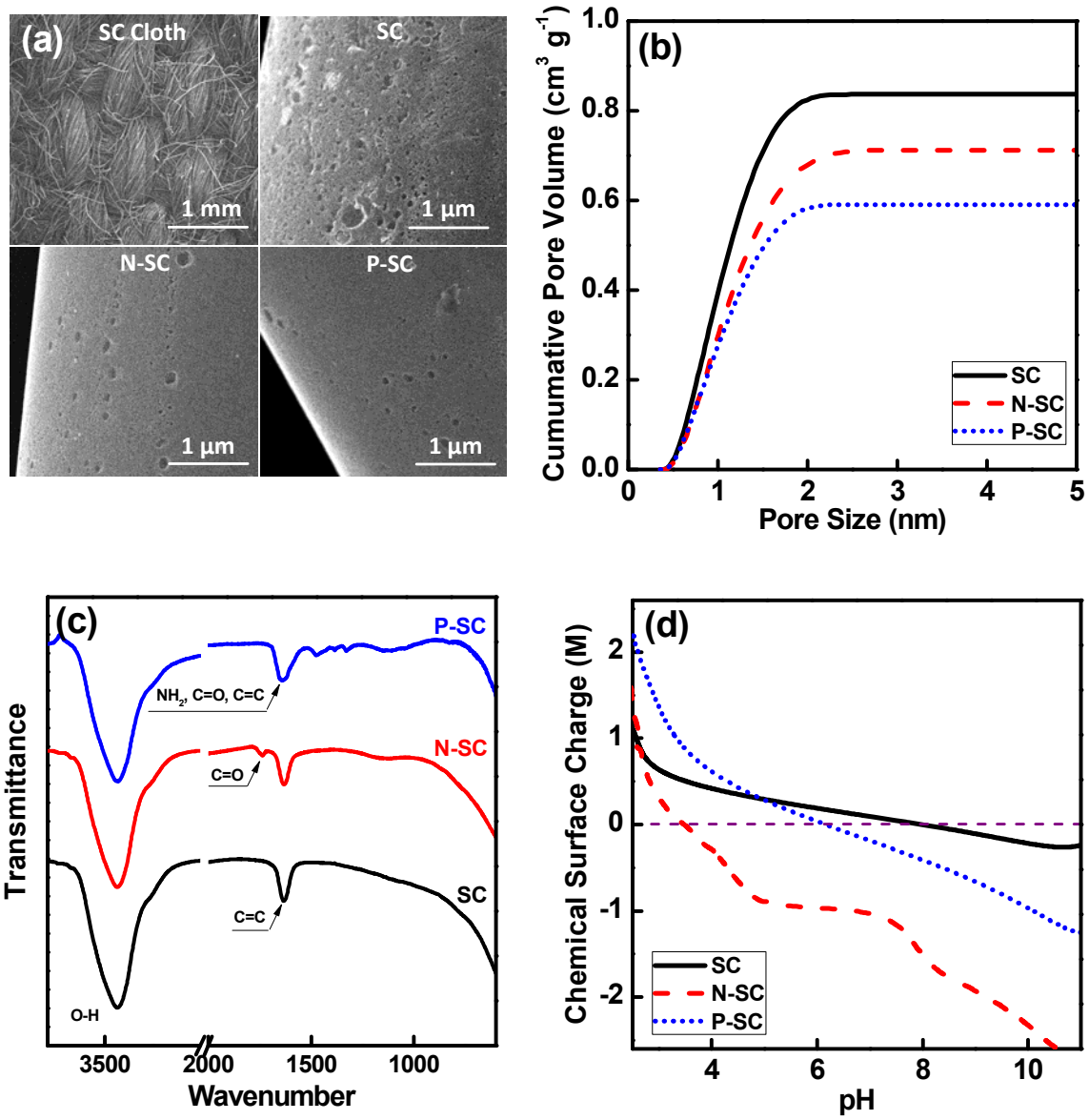

Figure 2. Physical and chemical characterizations of the treated and untreated carbon electrodes. (a) surface morphologies, (b) cumulative pore volumes, (c) surface chemical species, and (d) chemical surface charges of the SC, N-SC, and P-SC samples. The raw data such as the isotherms and titration results have been supplied in Fig. S1.

4. RESULTS AND DISCUSSION

In this work, carbon electrodes were synthesized with both negative and positive chemical surface charges and subsequently characterized using both physical and chemical methods. To validate a prediction generated from the amph-D model, these electrodes were incorporated into CDI cells for evaluation of their salt removal capability and their performance compared to that of untreated carbon electrodes. The following sections detail the physical and chemical properties of the carbon used in this study as well as their use for the removal of NaCl from solution.

4.1 Electrode Characterizations - Typical surface morphologies for the SC electrodes are seen in Fig. 2(a). The electrodes used in this study are composed of compact bundles of carbon fibers woven together, and this structure was maintained throughout the chemical treatments. Furthermore, carbon fibers in each sample generally have very similar physical structures, where many pores with micrometer ranges are found at the carbon fiber surface. In addition, the surface of the as-received SC fiber is usually much rougher compared to that of the treated samples. Changes in the total pore volume of the treated electrodes are reflected via gas adsorption and desorption tests. As shown in Fig. 2(b) for cumulative pore volumes, compared to the SC sample, the N-SC and P-SC pore volumes were reduced from around 0.82 mL g^{-1} to about 0.72 and 0.60 mL g^{-1}, respectively. However, distinct microporosity still remained for both N-SC and P-SC as suggested in their pore size distributions in Fig. S1.

For these treated samples, not only porosity but also surface chemical species are altered. Fig. 2(c) depicts typical FTIR spectra for the samples as expressed in terms of transmittance. In addition to O-H and C=C stretching vibrations found at 3430 and 1600

cm^{-1}, respectively, for all the samples, newly formed bands reveal modifications in the surface species of the SC after the chemical treatments. For instance, bands formed at 1730 and 1150 cm^{-1} in the N-SC spectrum denote C=O and C-O stretching, respectively. This assignment indicates that carboxylic groups (-COOH) are attached on the N-SC surface commensurate with region A in the amph-D model. In the P-SC spectrum, a broad band between 1660-1580 cm^{-1} presents overlapped signatures for C=O stretching, NH_2 scissoring, and C=C stretching.(Gao et al. 2015a) These characteristics indicate the formation of amine (-NH_2) and/or amide (-CO-NH-) functional groups, which has been documented elsewhere using similar treatments on carbon nanotubes and activated carbons.(Gao et al. 2015a, Longhi et al. 2006, Pan et al. 2006, Vuković et al. 2010) The presence of these overlapped signatures could correspond to both regions A and B in the amph-D model.

In a salt solution, functional groups (such as -COOH and -NH_2) can be either deprotonated or protonated, depending upon the solution's pH value.(Andreozzi et al. 2005, Gao et al. 2015a, Putra et al. 2009) These reactions result in fixed chemical charges being formed at electrode surfaces, behaving like ion-exchange membranes and further facilitating salt removal in CDI processes. To demonstrate changes in the chemical surface charge through the carbon treatments, chemical surface charge is plotted as a function of pH according to the potentiometric titration data in Fig. S1. As shown in Fig. 2(d), compared to the SC sample, enhancements in the chemical surface charge are observed in the P-SC and N-SC samples. In particular, the P-SC sample displays a very positive chemical surface charge at lower pH values. In contrast, the N-SC sample

reveals a much more negative chemical surface charge in the tested pH range, especially at higher pH values.

Finally, through these characterizations, values such as the pore volume and chemical surface charge will be shown together with the amph-D model to verify both the e-CDI and eV-CDI effects. To facilitate discussion in the following text, CDI cells formed with the untreated and treated SC electrodes are designated as “cell I” and “cell II”, respectively.

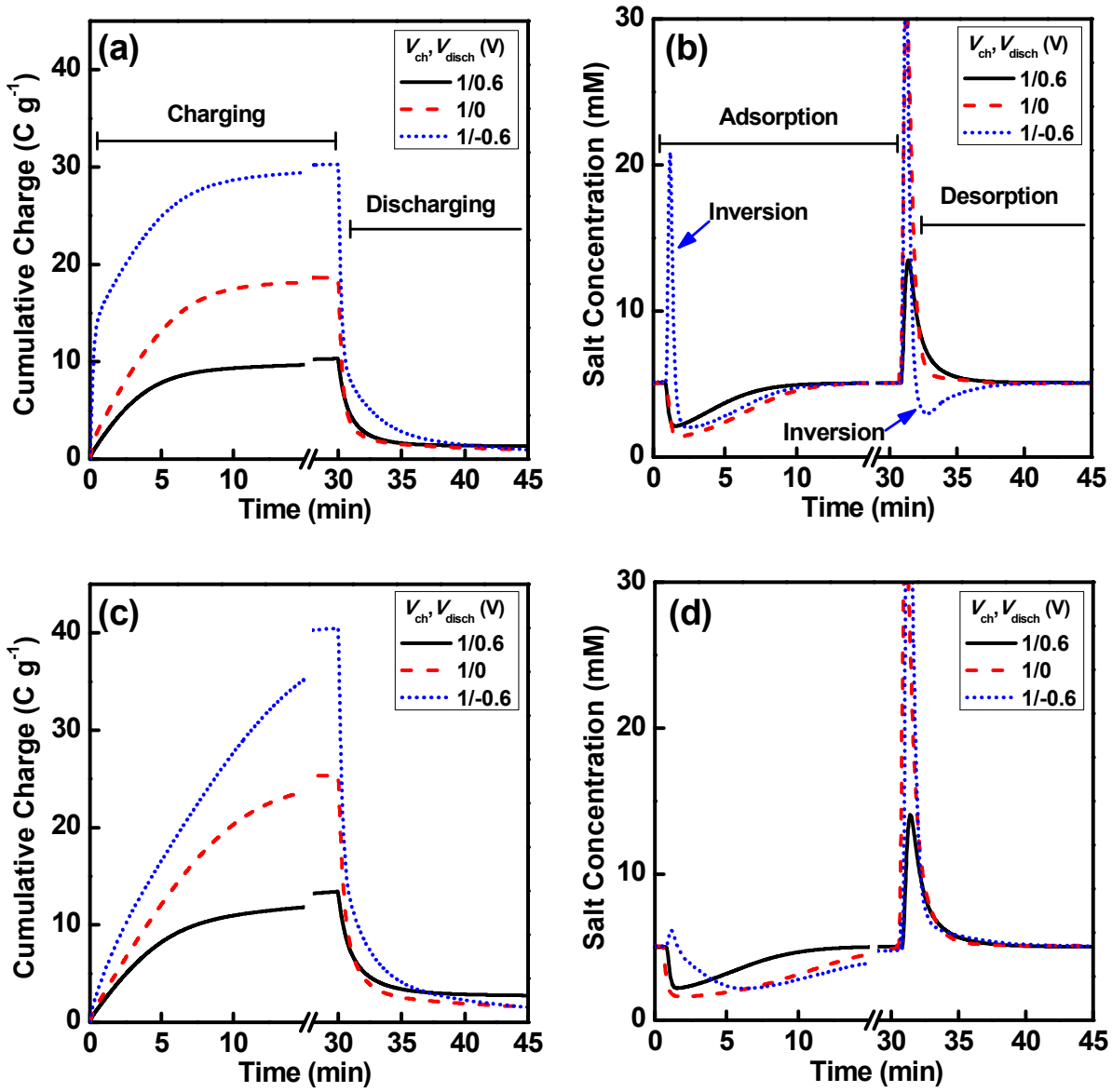

Figure 3. Cumulative charge and effluent salt concentration of a flow-by CDI cell using 5 mM deaerated NaCl solution at 15 mL min^{-1}. In this test, the charging voltage was fixed at 1.0 V while the discharge voltage was varied from 0.6, 0, and -0.6 V (1/0.6, 1/0, and

1/-0.6 V). Each charging and discharging step took 30 min. (a) and (b) cell I, and (c) and (d) cell II.

4.2 Cycling Performance - The characterized SC electrodes were used in a CDI cell. Fig. 3(a) and (b) depict cumulative charge and effluent salt concentration profiles for cell I at 1/0.6, 1/0, and 1/-0.6 V in 5 mM deaerated NaCl solution. Typical charge passed and salt removal patterns are formed at 1/0.6 and 1/0 V, in which salt adsorption is reflected by a decrease in the effluent concentration during charging while salt desorption is found with an increase in the effluent concentration during discharging. However, when the cell was operated at 1/-0.6 V, a distinct inversion peak and valley are highlighted at the beginning of charging and discharging, respectively. The inversion peak is attributed to salt adsorption during the previous discharging step. Similarly, the inversion valley is due to salt desorption during the previous charging step. In addition, the inversion feature detailed in this study describes the opposite functionality to a conventional CDI cell such as salt desorption during charging and salt adsorption during discharging. Details regarding the origin of this inversion will be provided later in the manuscript, i.e., Fig. 4.

Overall, cell I results in SAC values of 5.7, 9.6, and 4.3 mg g^{-1} with the corresponding total charges passed of 9.8, 19.0, and 31.0 C g^{-1} at 1/0.6, 1/0, and 1/-0.6 V, respectively. Under the same experimental conditions, in contrast to cell I, Fig. 3(c) and (d) display improved cumulative charge and effluent concentration profiles for cell II. For instance, the SAC values are boosted to 6.8, 15.4, and 16.7 mg g^{-1} with the respective total charges passed of 11.8, 25.9, and 41.6 C g^{-1} at 1/0.6, 1/0, and 1/-0.6 V, respectively.

Furthermore, the inverted behavior in Fig. 3(b) nearly disappears in Fig 3(d) when using the treated electrodes.

4.3 Interpretation of CDI Results - The results shown in Fig. 3 initiate an important topic related to the working voltage window of a CDI cell. As depicted in Fig. 4, this working voltage window is defined as the span between the charging voltage, V_{ch}, and discharge voltage, V_{disch}, i.e., $V_{ch} - V_{disch}$, where the charging and discharge voltages mean cell voltages during charging and discharging steps, respectively. The typical expectation is that an increase in the charging voltage of a CDI cell can boost salt removal. However, this increase will eventually be restricted by the potential for water splitting and carbon oxidization/decomposition,(Cohen et al. 2013) which is detrimental to the SAC and charge efficiency of a CDI cell. As a consequence, in order to extend the working voltage window of a CDI cell, an alternative is to lower the discharge voltage, e.g., below the short-circuit voltage.(Biesheuvel et al. 2016) In the following section, together with the amph-D model, this alternative will be illustrated in detail. In fact, improved salt removal due to a reduction in the discharge voltage has already been demonstrated in Fig. 3.

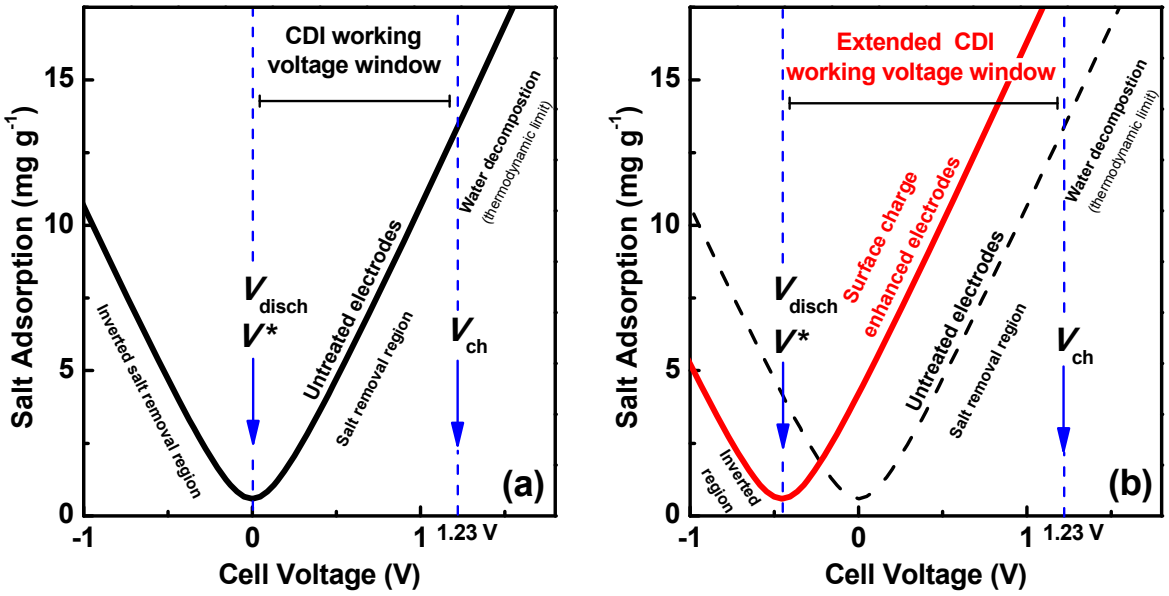

Figure 4. Predicted salt adsorption (SA) as a function of discharge voltage for CDI cells using (a) $\sigma_{chem,A} = \sigma_{chem,C} = 0$, i.e., untreated electrodes, and (b) $\sigma_{chem,A} = -\sigma_{chem,C} = 400$ mM, i.e., surface charge enhanced electrodes, where subscripts of A and C represent the anode and cathode, respectively. This prediction is carried out using the amph-D model with the same parameters as depicted in Fig. 1. SA differs from SAC introduced in Fig. 1, as SA is defined as the absolute amount of salt adsorbed at a certain cell voltage in a CDI cell, while SAC is described as the difference of two SA values, one at V_{ch} and another at V_{disch}.

As highlighted in Fig. 4, as function of the chemical surface charge of the carbon electrodes used in a CDI cell, the amph-D model predicts an important characteristic voltage, V^*, being the minimum of the curve of salt adsorption, SA, versus cell voltage. Mathematically, V^* is obtained from the hyperbolic function in Eq. [5]. Physically, V^*

indicates the discharge voltage at which a minimum adsorption, or maximum desorption of salt, thus the least SAC, occurs in a CDI cell. Similar understanding can be gained from the E_{PZC} for a single carbon electrode tested in a dilute salt solution (Bard and Faulkner 2001, Levi et al. 2013) because when a potential applied to a carbon electrode equals the E_{PZC}, the electrode has a least capacity for ion adsorption. In a CDI cell, there are always two values of E_{PZC}, one associated with the cathode and another with the anode. Indeed, these two values of E_{PZC} can theoretically be used in determining V^* in the amph-D model. This combination dramatically simplifies the mathematical description for a CDI cell, especially when the cathode and anode have different values of E_{PZC} or different chemical surface charges.

Following from the discussion above, it is apparent that V^* is a fundamental property of a CDI cell that can determine the extent of salt removal within the CDI working voltage window. For instance, as shown in Fig. 4(a), if the CDI cell is discharged below V^*, and charged at V^*, salt will be desorbed during charging and adsorbed during discharging, resulting in inverted CDI functionality. In contrast, if a CDI cell is charged above V^*, and then discharged at V^*, salt will be adsorbed during charging and desorbed during discharging, resulting in conventional CDI functionality. (It should be noted here that V_{ch} is always greater than V_{disch} according to Fig. 4.) As a consequence, in order to achieve the highest SAC value, a CDI cell should always be operated in a working voltage window such that the cell is discharged at V^* and charged just below the potential for water splitting and/or carbon decomposition.

Interestingly, with an increase of the chemical surface, the amph-D model predicts a gradual relocation of the V^* towards a lower voltage, see Fig. 4(b). This

negative shift in V^* only depends on the chemical surface charge conditions of the carbon electrodes used in a CDI cell (independent of CDI cell voltage). Therefore, it is understood in Fig. 1 that the use of surface charge enhanced electrodes can shift the V^* toward the negative direction (to a more negative cell voltage during discharge). This shifting results in a broadened working voltage window for a CDI cell, increasing the value of SAC due to both the e-CDI and eV-CDI effect.

To demonstrate both e-CDI and eV-CDI effects, cycling experiments were further performed using cell I and II again in 5 mM NaCl solution when both the CDI cells were charged at 1.0 V for 30 min and discharged from -1.0 to 0.6 V for another 30 min. (It should be noted that 1.0 V as a charging voltage was selected (and not a higher cell voltage) to avoid water splitting and minimize anode oxidation in the CDI cells.) Relevant results are summarized in Fig. 5 in terms of SAC and charge efficiency as a function of discharge voltage. As shown in Fig. 5(a), the experimental values for SAC (symbols) are very similar to the prediction generated by the amph-D model in Fig. 1, presenting a maximum SAC at a discharge voltage of 0 and -0.4 V for cell I and II, respectively. As illustrated earlier for the eV-CDI effect, this negatively extended discharge voltage should be primarily attributed to the chemical surface charge enhanced electrodes configured in cell II, broadening the total working voltage window from 1.0 to 1.4 V based upon these two CDI cells. Correspondingly, the maximum SAC value increases from 9.6 to 17.1 mg g^{-1}.

In the CDI literature, it is commonly thought that reduced pore volumes for carbon electrodes primarily lead to a lower SAC value.(Porada et al. 2013) Therefore, it would be expected that the SAC values associated with cell I would be greater than those

for cell II since the carbon electrodes in cell II have diminished pore volumes according to Fig. 2(b). However, as shown in Fig. 5(a), it is the other way around, and the SAC values for cell I are always smaller than those for cell II at the same charging/discharge voltage. For instance, at a typical discharge voltage of 0 V, the SAC value is enhanced from 9.6 mg g^{-1} for cell I to 15.4 mg g^{-1} for cell II. This enhanced SAC can be interpreted by the e-CDI effect, which is fundamentally due to the surface charge enhanced electrodes used in cell II. Thus, it is believed that to design carbon electrodes for CDI applications, in addition to the pore size distribution, surface charge also plays a central role in CDI cells, as underpinned theoretically by the amph-D model.

As shown in Fig. 5(b), a decrease in the discharge voltage leads to a decrease in charge efficiency for both CDI cells. This reduced charge efficiency is mainly accounted for by the inverted salt removal (or salt repulsion) depicted in Fig. 3(b), which occurs when the discharge voltage is more negative than V^*. Furthermore, cell II generally shows higher charge efficiency at each discharge voltage compared to cell I. This improved charge efficiency should be due to the negative shifting of V^* by using the surface charge enhanced electrodes. As discussed earlier, V^* is related to the E_{PZC} associated with both the cathode and anode. Therefore, this type of behavior can also be interpreted based upon the knowledge regarding E_{PZC}, which can be found in a CDI case study in ref. (Gao et al. 2015a).

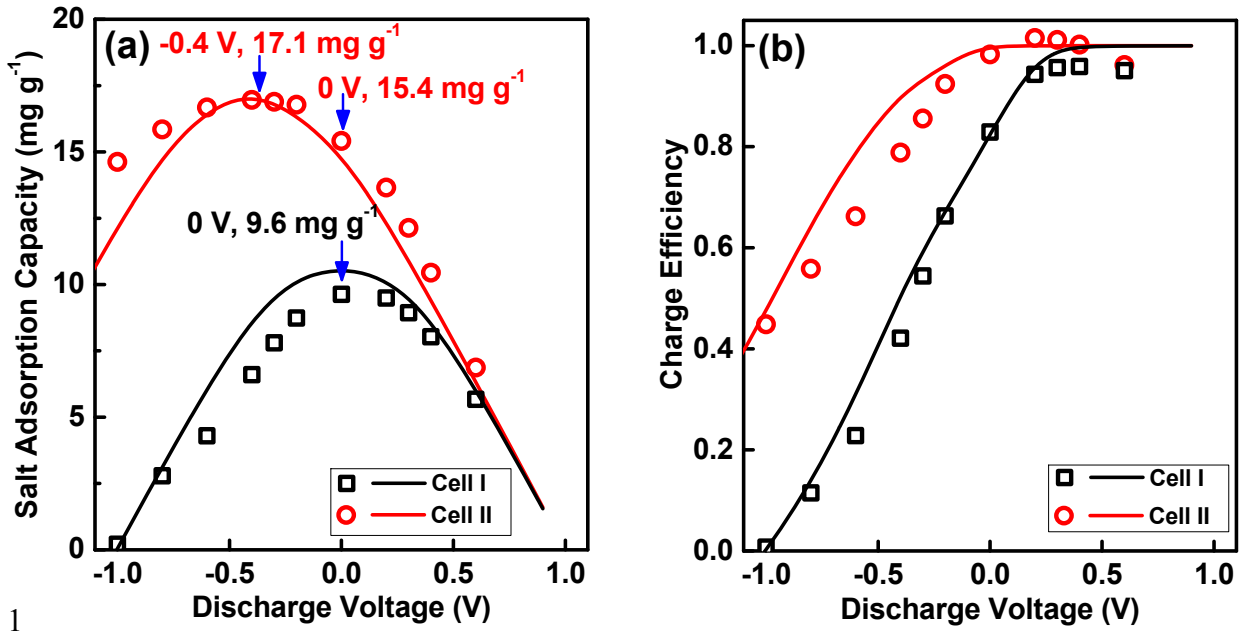

Figure 5. (a) Salt adsorption capacity and (b) charge efficiency as a function of discharge voltage for cell I and II. In these experiments, the CDI cells were charged at 1.0 V for 30 min and discharged at different voltages for another 30 min. In these plots, symbols represent the experimental results obtained from cycling experiments, and lines denote the theoretical results calculated by the amph-D model using the fitting parameters in Table 1. In addition, charge passed as a function of discharge voltage has been plotted in Fig. S2.

To further demonstrate application of the amph-D model in describing the effect of chemical surface charge in CDI, several fitting parameters are selected to construct the theoretical lines via the equations introduced in the theory section. (It should be noted here that the fitting parameters for the pore volume are collected from the experimental results.) It can be seen that the selected fitting parameters given in Table 1 give results that are in reasonable agreement to both the experimentally obtained SAC and charge

efficiency values. However, in comparison to the measured chemical surface charge by the potentiometric titrations in Fig. 2(d), to fit the data, the theory requires lower values for the chemical surface charge than measured, especially for the cathode (N-SC). This discrepancy suggests that (1) not all functional groups may be accessible or active in CDI, and (2) the local pH in the micropores may be more extreme than that outside the electrodes when potentials were applied to the electrodes, reducing the ionization degree of the charges. Nevertheless, the titration performed in this study demonstrates a relevant method to estimate the presence and concentration of surface groups, which can be referenced and used for future studies regarding CDI electrodes.

Finally, we observe that the magnitude of the fitting parameters (such as pore volume and chemical surface charge) generally agrees with the experimental characterizations depicted in Fig 2. As a result, it is believed that these simple experimental methods (such as gas adsorption/desorption and titration) are appropriate for the characterization of electrodes for CDI applications.

Table 1. Fitting parameters used in the amph-D model to plot the theoretical results shown in Fig. 5. A and B represent region A and B, respectively, and we assume $\alpha = 0.5$. The values in the second row for cell II are the additional surface charges due to the use of surface charge enhanced electrodes. The pore volumes are obtained from Fig. 2(b). The Stern capacitance is very typical for the Donnan model in CDI,(Dykstra et al. 2016) which also matches the values reported in the field of EDL-capacitors.

	Cell I	Cell II

	Anode (P-SC)		Cathode (N-SC)		Anode (P-SC)		Cathode (N-SC)	
Chemical Surface Charge, σ (M)	A	B	A	B	A	B	A	B
	-0.20	0.20	-0.20	0.20	-0.20 +0.55	0.20 +0.55	-0.20 -0.25	0.20 -0.25
Pore Volume, v_{mi} (mL g^{-1})	0.82				0.60		0.72	
Stern Capacitance, C_s (F mL^{-1})	135							

5. CONCLUSIONS

In this study, both experimental and theoretical methods were applied to understand changes in salt removal in a CDI cell. Improved salt removal due to a reduction in discharge voltage was clearly demonstrated using both untreated and treated (surface charge enhanced) carbon electrodes. This demonstration is for the first time validating both the e-CDI and eV-CDI effects predicted by the amph-D model, which states that in addition to the pore size distribution of the carbon electrode, carbon surface chemistry also lies at the foundation of salt removal in CDI cells.

Following from the above-mentioned conclusions, it is considered that both the carbon's pore size distribution and chemical surface charge should be optimized when

designing novel/new carbon electrodes for CDI applications, including membrane-assisted, flow-electrode, and inverted CDI cells. These two parameters can be simply measured by gas adsorption/desorption, potentiometric titration, cyclic voltammetry and electrochemical impendence spectroscopic techniques, and from the resulting pore volume, chemical surface charge and E_{PZC}, together with the amph-D model, it is possible to properly predict the salt adsorption capacity, charge passed, and charge efficiency for CDI cells.

ACKNOWLEDGEMENT

These authors are grateful to the U.S. - China Clean Energy Research Center, U.S. Department of Energy for project funding (No. DE-PI0000017). Part of this work was performed in the cooperation framework of Wetsus, European Centre of Excellence for Sustainable Water Technology (www.wetsus.eu). Wetsus is co-funded by the Dutch Ministry of Economic Affairs and Ministry of Infrastructure and Environment, the Province of Fryslân, and the Northern Netherlands Provinces.

REFERENCES

Anderson, M.A., Cudero, A.L. and Palma, J., 2010. Capacitive deionization as an electrochemical means of saving energy and delivering clean water. Comparison to present desalination practices: Will it compete? *Electrochim. Acta* 55(12), 3845-3856.

Andreozzi, R., Canterino, M., Marotta, R. and Paxeus, N., 2005. Antibiotic removal from wastewaters: The ozonation of amoxicillin. *J. Hazard. Mater.* 122(3), 243-250.

Avlonitis, S., Kouroumbas, K. and Vlachakis, N., 2003. Energy consumption and membrane replacement cost for seawater RO desalination plants. *Desalination* 157(1), 151-158.

Avraham, E., Noked, M., Cohen, I., Soffer, A. and Aurbach, D., 2011. The Dependence of the Desalination Performance in Capacitive Deionization Processes on the Electrodes PZC. *J. Electrochem. Soc.* 158(12), P168-P173.

Babić, B.M., Milonjić, S.K., Polovina, M.J. and Kaludierović, B.V., 1999. Point of zero charge and intrinsic equilibrium constants of activated carbon cloth. *Carbon* 37(3), 477-481.

Bard, A.J. and Faulkner, L.R., 2001. Electrochemical Methods - Fundamentals and Applications, John Wiley & Sons, New York.

Bian, Y., Yang, X., Liang, P., Jiang, Y., Zhang, C. and Huang, X., 2015. Enhanced desalination performance of membrane capacitive deionization cells by packing the flow chamber with granular activated carbon. *Water Res.* 85, 371-376.

Biesheuvel, P.M., 2015. Activated carbon is an electron-conducting amphoteric ion adsorbent. arXiv preprint arXiv:1509.06354.

Biesheuvel, P.M., Hamelers, H.V.M. and Suss, M.E., 2016. Theory of water desalination by porous electrodes with fixed chemical charge. *Colloid. Interf. Sci. Commun.* 10.1016/j.colcom.2015.12.001.

Biesheuvel, P.M., Porada, S., Levi, M. and Bazant, M.Z., 2014. Attractive forces in microporous carbon electrodes for capacitive deionization. *J. Solid State Electrochem*. 18(5), 1365-1376.

Biesheuvel, P.M., Suss, M.E. and Hamelers, H.V.M., 2015. Theory of water desalination by porous electrodes with fixed chemical charge. arXiv preprint arXiv:1506.03948.

Blair, J. and Murphy, G., 1960. SALINE WATER CONVERSION, pp. 206-223, American Chemical Society.

Boehm, H.P., 1994. Some aspects of the surface chemistry of carbon blacks and other carbons. *Carbon* 32(5), 759-769.

Bouhadana, Y., Avraham, E., Noked, M., Ben-Tzion, M., Soffer, A. and Aurbach, D., 2011. Capacitive deionization of NaCl solutions at non-steady-state conditions: inversion functionality of the carbon electrodes. *J. Phys. Chem. C* 115(33), 16567-16573.

Cohen, I., Avraham, E., Bouhadana, Y., Soffer, A. and Aurbach, D., 2013. Long term stability of capacitive de-ionization processes for water desalination: The challenge of positive electrodes corrosion. *Electrochim. Acta* 106, 91-100.

Cohen, I., Avraham, E., Noked, M., Soffer, A. and Aurbach, D., 2011. Enhanced Charge Efficiency in Capacitive Deionization Achieved by Surface-Treated Electrodes and by Means of a Third Electrode. *J. Phys. Chem. C* 115(40), 19856-19863.

Duan, F., Du, X., Li, Y., Cao, H. and Zhang, Y., 2015. Desalination stability of capacitive deionization using ordered mesoporous carbon: Effect of oxygen-containing surface groups and pore properties. *Desalination* 376, 17-24.

Dykstra, J., Zhao, R., Biesheuvel, P. and van der Wal, A., 2016. Resistance identification and rational process design in Capacitive Deionization. *Water Res.* 88, 358-370.

Elimelech, M. and Phillip, W.A., 2011. The future of seawater desalination: energy, technology, and the environment. *Science* 333(6043), 712-717.

Farmer, J.C., Fix, D.V., Mack, G.V., Pekala, R.W. and Poco, J.F., 1996. Capacitive Deionization of NaCl and NaNO3 Solutions with Carbon Aerogel Electrodes. *J. Electrochem. Soc.* 143(1), 159-169.

Gao, X., Omosebi, A., Landon, J. and Liu, K., 2014. Dependence of the Capacitive Deionization Performance on Potential of Zero Charge Shifting of Carbon Xerogel Electrodes during Long-Term Operation. *J. Electrochem. Soc.* 161(12), E159-E166.

Gao, X., Omosebi, A., Landon, J. and Liu, K., 2015a. Enhanced Salt Removal in an Inverted Capacitive Deionization Cell Using Amine Modified Microporous Carbon Cathodes. *Environ. Sci. Tech.* 49(18), 10920-10926.

Gao, X., Omosebi, A., Landon, J. and Liu, K., 2015b. Surface charge enhanced carbon electrodes for stable and efficient capacitive deionization using inverted adsorption-desorption behavior. Energy Environ. Sci. 8(3), 897-909.

Gendel, Y., Rommerskirchen, A.K.E., David, O. and Wessling, M., 2014. Batch mode and continuous desalination of water using flowing carbon deionization (FCDI) technology. *Electrochem. Commun.* 46(0), 152-156.

Hatzell, K.B., Iwama, E., Ferris, A., Daffos, B., Urita, K., Tzedakis, T., Chauvet, F., Taberna, P.-L., Gogotsi, Y. and Simon, P., 2014. Capacitive deionization concept based on suspension electrodes without ion exchange membranes. *Electrochem. Commun.* 43(0), 18-21.

Jande, Y.A.C. and Kim, W.S., 2013. Desalination using capacitive deionization at constant current. *Desalination* 329, 29-34.

Junjie, Y., Shufeng, S., Jinhua, W. and Jiping, L., 2007. Improvement of a multi-stage flash seawater desalination system for cogeneration power plants. *Desalination* 217(1), 191-202.

Lee, J., Kim, S., Kim, C. and Yoon, J., 2014. Hybrid capacitive deionization to enhance the desalination performance of capacitive techniques. *Energy Environ. Sci.* 7(11), 3683-3689.

Leon y Leon, C.A., Solar, J.M., Calemma, V. and Radovic, L.R., 1992. Evidence for the protonation of basal plane sites on carbon. *Carbon* 30(5), 797-811.

Levi, M.D., Sigalov, S., Aurbach, D. and Daikhin, L., 2013. In Situ Electrochemical Quartz Crystal Admittance Methodology for Tracking Compositional and Mechanical Changes in Porous Carbon Electrodes. *J. Phys. Chem. C* 117(29), 14876-14889.

Longhi, M., Bertacche, V., Bianchi, C.L. and Formaro, L., 2006. Preparation and Characterization of Aminated Carbon from a Single-Step Reaction. *Chem. Mater.* 18(17), 4130-4136.

McCafferty, E., 2010. Relationship between the isoelectric point (pHpzc) and the potential of zero charge (Epzc) for passive metals. *Electrochim. Acta* 55(5), 1630-1637.

Montes-Morán, M.A., Suárez, D., Menéndez, J.A. and Fuente, E., 2004. On the nature of basic sites on carbon surfaces: an overview. *Carbon* 42(7), 1219-1225.

Noh, J.S. and Schwarz, J.A., 1990. Effect of HNO3 treatment on the surface acidity of activated carbons. *Carbon* 28(5), 675-682.

Omosebi, A., Gao, X., Rentschler, J., Landon, J. and Liu, K., 2015. Continuous operation of membrane capacitive deionization cells assembled with dissimilar potential of zero charge electrode pairs. *J. Colloid Interf. Sci.* 446(0), 345-351.

Oren, Y. and Soffer, A., 1978. Electrochemical Parametric Pumping. *J. Electrochem. Soc.* 125(6), 869-875.

Pan, B., Cui, D., Gao, F. and He, R., 2006. Growth of multi-amine terminated poly (amidoamine) dendrimers on the surface of carbon nanotubes. *Nanotechnology* 17(10), 2483.

Porada, S., Borchardt, L., Oschatz, M., Bryjak, M., Atchison, J.S., Keesman, K.J., Kaskel, S., Biesheuvel, P.M. and Presser, V., 2013. Direct prediction of the desalination performance of porous carbon electrodes for capacitive deionization. *Energy Environ. Sci.* 6(12), 3700-3712.

Putra, E.K., Pranowo, R., Sunarso, J., Indraswati, N. and Ismadji, S., 2009. Performance of activated carbon and bentonite for adsorption of amoxicillin from wastewater: Mechanisms, isotherms and kinetics. *Water Res.* 43(9), 2419-2430.

Schwarzenbach, R.P., Egli, T., Hofstetter, T.B., Von Gunten, U. and Wehrli, B., 2010. Global water pollution and human health. *Annu. Rev. Environ. Resour.* 35, 109-136.

Seo, S.-J., Jeon, H., Lee, J.K., Kim, G.-Y., Park, D., Nojima, H., Lee, J. and Moon, S.-H., 2010. Investigation on removal of hardness ions by capacitive deionization (CDI) for water softening applications. *Water Res.* 44(7), 2267-2275.

Subramani, A. and Jacangelo, J.G., 2015. Emerging desalination technologies for water treatment: A critical review. *Water Res.* 75(0), 164-187.

Suss, M.E., Baumann, T.F., Bourcier, W.L., Spadaccini, C.M., Rose, K.A., Santiago, J.G. and Stadermann, M., 2012. Capacitive desalination with flow-through electrodes. *Energy Environ. Sci.* 5(11), 9511-9519.

Suss, M.E., Porada, S., Sun, X., Biesheuvel, P.M., Yoon, J. and Presser, V., 2015. Water desalination via capacitive deionization: what is it and what can we expect from it? *Energy Environ. Sci.* 8(8), 2296-2319.

Tang, W., Kovalsky, P., He, D. and Waite, T.D., 2015. Fluoride and nitrate removal from brackish groundwaters by batch-mode capacitive deionization. *Water res.* 84, 342-349.

Vuković, G.D., Marinković, A.D., Čolić, M., Ristić, M.Đ., Aleksić, R., Perić-Grujić, A.A. and Uskoković, P.S., 2010. Removal of cadmium from aqueous solutions by oxidized and ethylenediamine-functionalized multi-walled carbon nanotubes. *Chem. Eng. J.* 157(1), 238-248.

Wu, T., Wang, G., Dong, Q., Qian, B., Meng, Y. and Qiu, J., 2015. Asymmetric capacitive deionization utilizing nitric acid treated activated carbon fiber as the cathode. *Electrochimi. Acta* 176, 426-433.

Yang, J., Zou, L. and Choudhury, N.R., 2013. Ion-selective carbon nanotube electrodes in capacitive deionisation. *Electrochim. Acta* 91(0), 11-19.

Zhao, R., Biesheuvel, P.M., Miedema, H., Bruning, H. and van der Wal, A., 2010. Charge Efficiency: A Functional Tool to Probe the Double-Layer Structure Inside of Porous Electrodes and Application in the Modeling of Capacitive Deionization. *J. Phys. Chem. Lett.* 1(1), 205-210.

Zhao, R., Satpradit, O., Rijnaarts, H.H.M., Biesheuvel, P.M. and van der Wal, A., 2013. Optimization of salt adsorption rate in membrane capacitive deionization. *Water Res.* 47(5), 1941-1952.